Interspecies interaction controls *Escherichia coli* growth in human gut microbiome samples

Mathilde Boumasmoud[1*], Ricardo León-Sampedro[1,2], Vera Beusch[1], Fabienne Benz[1,3], Markus Arnoldini[4] and Alex R. Hall[1]

1 Institute of Integrative Biology, Department of Environmental Systems Science, ETH Zurich, Zurich, Switzerland
2 Biomedical Research Networking Center for Epidemiology and Public Health (CIBERESP), Spain
3 Institut Pasteur, Université Paris Cité, CNRS UMR6047, Synthetic Biology, Paris 75015, France
4 Department of Health Science and Technology, ETH Zurich, Zurich, Switzerland
*Corresponding author: mathilde.boumasmoud@env.ethz.ch

Abstract

Gut microbial community composition varies from one person to another. Potentially, this means the ecological interactions experienced by individual strains or species also vary among microbiomes of different people. However, testing this directly in human microbiomes and identifying ecological drivers involved is challenging. Here, we use replicated anaerobic microcosms to quantify variability of population growth for a key commensal species among microbiome samples from different individuals, and to identify underlying intra- and interspecific interactions. In a reciprocal transplant experiment, both absolute and relative growth performance of different *Escherichia coli* strains varied among gut microbiome samples from healthy individuals. This was partly explained by intraspecific competition: ecological success of individual *E. coli* strains was associated with displacement of resident conspecifics. However, the determinants of *E. coli* growth varied among samples. In one microbiome sample with a distinctive taxonomic composition, culture acidification by resident microbes impaired growth of all *E. coli* strains. We identified a strain of *Clostridium butyricum* contributing to this effect, and showed that transferring it into other microbiomes predictably altered pH, fermentation product profiles (butyrate accumulation and acetate/lactate depletion) and population growth of other species including *E. coli*, thereby reshaping overall taxonomic composition. Our results suggest natural inter-individual gut microbiome variation translates to variable ecological interactions with incoming bacteria, but these dynamics can be manipulated by a generalizable interspecies interaction.

Significance statement

Gut-microbiome variation among healthy individuals is widely documented, yet its impact on the success of incoming bacterial strains and its implications for microbiome-targeted interventions remain unclear. Here, we test this experimentally by cultivating stool samples from healthy individuals and transplanting strains across samples. We reveal a functional relationship between microbiome variation and growth performance of individual strains. This underscores the challenge of predicting colonization outcomes. Yet, we identify a taxon contributing to the distinct functional profile of one of the samples, and show that its transplantion into other microbiome samples reproducibly alters key properties, including pH and population growth of other bacteria, revealing a common ecological control point. These findings advance our ability to explain and manipulate human gut-microbiome variation.

Introduction

Microbial colonization of the human gastrointestinal tract begins at birth [1]. After a dynamic development during the first years of life [2], microbial community composition remains relatively stable, with changes mostly in the relative abundances of different taxa [3]. Within individual subjects, resident strains can be retained for extended periods [4,5] but also occasionally replaced by newly-arriving strains [6,7]. Among individual subjects, taxonomic composition of the gut microbiota is highly individual, as evidenced by community profiles from 16S rRNA amplicon sequencing and analyses at the strain-level [8]. This variation among microbiomes of different individuals, shaped by host and environmental factors [2,9], may itself be a key determinant of who becomes colonized by which newly incoming strain, both early on in life and during later strain turnover. In support of this idea, various mechanisms have been identified by which interactions with resident microbiota can affect population growth of individual strains, such as nutrient competition [10], crossfeeding [11] and direct inhibition [12]. Thus, variable taxonomic composition may result in variation of these ecological interactions and, in turn, variable population growth of incoming strains. Experiments in mice support this idea: colonization success for the same strain can vary across different microbiomes [13]. Furthermore, different strains within a given species often have different phenotypes relevant for colonisation, such as nutrient preferences [14]. Some of these strain-specific traits may be advantageous in some microbiomes but not in others. This means that inter-individual microbiome variation may determine both the relative performance of different strains within species, and average population growth at the species level.

Here, we quantify variation in population growth of the key gut commensal *Escherichia coli* across gut microbiome samples from different healthy individuals, including a resident microbiota and abiotic components [15]. First, we focus on the strain level to ask how absolute and relative performance of different strains varies among microbiome samples. Quantifying this variability is important for understanding the ecological determinants of strain diversity. For example, if relative performance of different strains varies among samples from different people, then microbiome-to-microbiome variation may be a key determinant of colonisation success for incoming strains and subsequent turnover. Furthermore, if the identity of the best-performing strain varies among microbiome samples, a pattern of local adaptation could emerge [16,17]. Despite many tests in other organisms, including plants and animals [18–20], and microbes in other ecosystems [21–25], it remains unclear whether such patterns apply to bacteria in human microbiomes. Second, we focus on the species level and ask what type of bacterial interactions explain variable average population growth of *E. coli* among microbiome samples from different individuals. Like many other species, *E. coli* naturally makes up a variable proportion of resident microbiota [26], raising the question of whether its abundance in a given microbiome is strongly influenced by interactions with particular taxa [27]. This aspect is relevant in the context of potential microbiome-based therapies, such as probiotics and fecal microbiota transplantation [28,29]. For instance, if growth of a focal species is strongly affected by interactions with one or a few other taxa, its abundance could potentially be manipulated therapeutically by inhibiting or introducing such relevant taxa [30]. By contrast, effects arising from complex interactions among several strains or species would be harder to manipulate predictably, requiring a more personalised approach instead [31].

Addressing these questions directly in human microbiomes and identifying the underlying ecological drivers is challenging. There have been major advances on related questions from work with synthetic communities in microcosms or gnotobiotic hosts [32–35]. However, the genetic variation within artificial communities, and differences among experimental groups in such systems, are not reflective of natural human-associated communities or real-world person-to-person variation. For example, the set of strains in an assembled community is typically not as species-rich and does not share the same history of ecological interactions as a natural community. Similarly, experiments with mice and associated microbiota have produced important insights [13,36], but leave gaps in our understanding of human-associated communities [37,38]. An important practical obstacle is that it is extremely challenging to measure the population growth of individual strains in the gut microbiomes of healthy individuals, let alone to do so under replicated introductions of the same strain set into the same microbiomes. We circumvent some of these challenges by using anaerobic microcosms constituted from fecal microbiome samples of healthy humans [39]. This enabled us to perform a reciprocal transplant experiment [16], measuring growth performance of six commensal *E. coli* isolates across the microbiome samples they were isolated from. Thus, we quantify the contribution of strain-to-strain and microbiome-to-microbiome differences to the 'ecological success' of commensal *E. coli*, interpreting ecological success or performance as the capacity to reach high abundance in the presence of a resident microbiota. We then investigate the underlying intra- and interspecies interactions and identify a single taxon capable of consistently altering the functional profile of different microbiome samples, thereby controlling growth of other bacteria including *E. coli*.

Results

Resident microbiota drive strain-specific *E. coli* performance across microbiome samples from different individuals

We sampled gut microbiomes from the stool of six healthy humans and from each we isolated a single *Escherichia coli* clone, representative of the most abundant resident *E. coli* strain (see Methods, Supplementary Fig. 1). We then inoculated these six focal strains, tagged with a selective marker, into anaerobic microcosms prepared with each of the six microbiome samples resuspended in a basal medium, generating 36 unique focal strain-microbiome combinations. Within 24 h, all focal strains reached high abundance (Fig. 1a). However, their final abundance varied both among focal strains and among microbiome samples from different individuals ($F_{5,72}$=27.4, $p < 0.001$ and $F_{5,72}$=15.0, $p < 0.001$ respectively in a two-way ANOVA, Fig. 1a). Furthermore, the relative performance of different focal strains depended on the microbiome context (interaction term, $F_{25,72}$=2.2, p=0.005). In some microbiome samples, such as M3, strain-to-strain differences were large, whereas in others, such as M6, strains performed more similarly. Despite these differences in the magnitude of variation, the rank order of strain performance was generally consistent across microbiome samples, with strains S3 and S7 generally reaching the highest abundances (Fig. 1a). Testing for evidence of local adaptation revealed no average difference between sympatric and allopatric strain-microbiome combinations (Supplementary Fig. 2a). Thus, some focal strains were generally more successful than others in terms of population growth in microcosms with a resident microbiota, but the strength of these differences and average ecological success varied across microbiome samples from different individuals.

To test for evidence that variable performance of *E. coli* in microbiome samples was linked to interactions between focal strains and resident microbiota, we performed an experiment equivalent to that above, but with sterilized versions of the same microbiome samples (hereafter, 'sterile' microcosms, as opposed to 'live' microcosms in the main experiment above). Here, all focal strains reached high abundance in all sterile microcosms (>10^8 CFU/mL, Fig. 1b). Relative performance of different focal strains was stable among sterilized microbiome samples (interaction term $F_{25,72}$=0.86, p=0.66), and the range of final abundances was smaller than in the experiment above with live microcosms (ranging from 1.7×10^8 to 5.9×10^8 CFU/mL vs. 9.7×10^6 to 5.9×10^8 CFU/mL). We also found no evidence of local adaptation in these conditions (Supplementary Fig. 2b). Nevertheless, we still found average differences among focal strains and sterilized microbiome samples ($F_{5,72}$= 9.2, $p < 0.001$ and $F_{5,72}$=3.1, p=0.012 respectively). There was no overall association between final abundances in sterile microcosms and in live microcosms (R=0.25, p=0.15, Supplementary Fig. 3), suggesting the drivers of focal strain performance were different in the presence versus absence of resident microbiota. In summary, the contrast between the large variability observed in live microcosms (Fig. 1a) and the invariably high abundances across strain-microbiome combinations in sterile microcosms (Fig. 1b) supports a critical role of the resident microbiota in determining strain-specific performance across microbiome samples from different individuals.

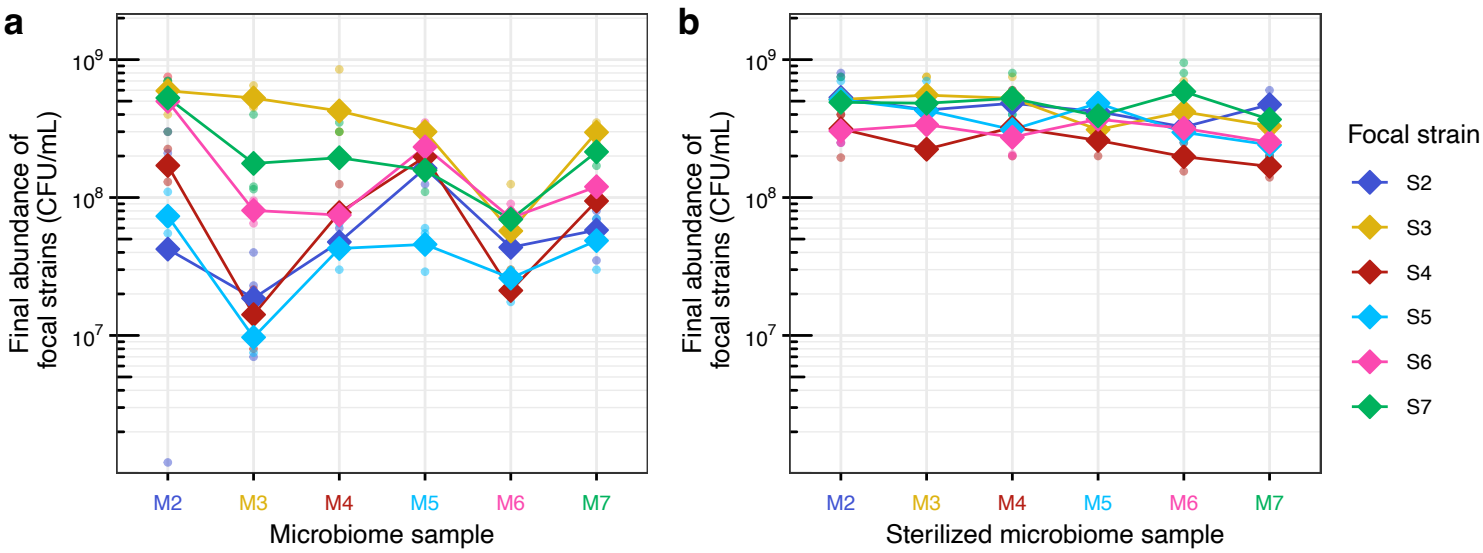

Fig. 1: Growth performance of focal *E. coli* strains in human gut microcosms. Final abundance of each focal *E. coli* strain (S2-S7) in microcosms prepared with each microbiome sample (M2-M7) live (a) or sterilized (b), estimated by selective plating after 24h of anaerobic incubation. Diamonds represent the average (geometric mean) of three replicates for each strain-microbiome combination and dots show individual replicates. Lines connect the average for each strain across microbiome samples. Colors of focal strains are matched to the color of their microbiome of origin (e.g., strain 3, S3, was isolated originally from microbiome sample 3, M3).

Intraspecific competition shapes strain performance within microbiome-specific finite *E. coli* abundance

We next tested for further evidence of interactions between focal strains and resident microbiota. First, we focused on their interactions with resident *E. coli* in each microbiome sample. Total *E. coli* abundance (including focal strain and resident *E. coli*) in live microcosms varied among samples from different individuals ($F_{5,72}$= 76.7, $p < 0.001$, Fig. 2a). Within each microbiome sample, total *E. coli* abundance was unaffected by focal strain identity ($F_{5,72}$= 1.3, p= 0.25, main panel Fig. 2a), despite considerable variation in focal strain performance (Fig. 1a). For example, in sample M3, average focal strain abundance ranged from 9.7×10^6 to 5.3×10^8 CFU/mL (Fig. 1a), but total *E. coli* abundance was relatively stable (ranging from 4.0×10^8 to 7.5×10^8 CFU/mL, main panel Fig. 2). This stability shows that focal strains achieving higher abundance did not increase overall *E. coli* load but displaced resident *E. coli*, indicating a microbiome-specific finite abundance for this species. Taking focal strain abundance as a proportion of the total *E. coli* population in each microcosm revealed that two strains (S3 and S7) consistently reached a comparable or greater abundance than resident *E. coli* (insets Fig. 2). Furthermore, in the respective microbiome samples of these two strains (M3 and M7, where the original untagged strains S3 and S7 are the most abundant resident *E. coli* strain; see Methods), all other focal strains reached relatively low frequencies (insets Fig. 2). This pattern supports the idea that in gut microcosms, S3 and S7 coexisted without strongly affecting each other, while suppressing other *E. coli* strains. The observed strain differences could potentially be explained by variable growth capacities in abiotic conditions, but we found no evidence for this: S3 and S7 showed no advantage in pure culture or pairwise competition in the basal medium used to prepare the microcosms (Supplementary Figs. 4 and 5), nor did they exhibit a particularly broad niche across 95 single-carbon-source conditions (Supplementary Figs. 6 and 7). In contrast, we found some evidence consistent with a role for direct antagonistic interactions between competing *E. coli* strains: S3 and S7 showed inhibitory activity

159 against some other strains on agar (Supplementary Figs. 8 and 9). This phenotype was associated with carriage
160 of a ColE1 plasmid encoding colicin E1 and the corresponding immunity gene. Transfer of the ColE1 plasmid to
161 a susceptible strain (S2) conferred immunity and inhibitory capacity on agar (Supplementary Fig. 10). However,
162 this did not enhance growth performance of S2 in live microbiomes (Supplementary Fig. 11a). This shows genetic
163 elements encoding bacteriocin-mediated antagonism are circulating among resident *E. coli* strains and may
164 contribute to strain-level performance, although the net effects were weak in this manipulation experiment in
165 a distinct genetic background. In summary, strain performance was constrained by a microbiome-specific finite
166 *E. coli* abundance and by intraspecific competition independent of intrinsinc growth capacities.

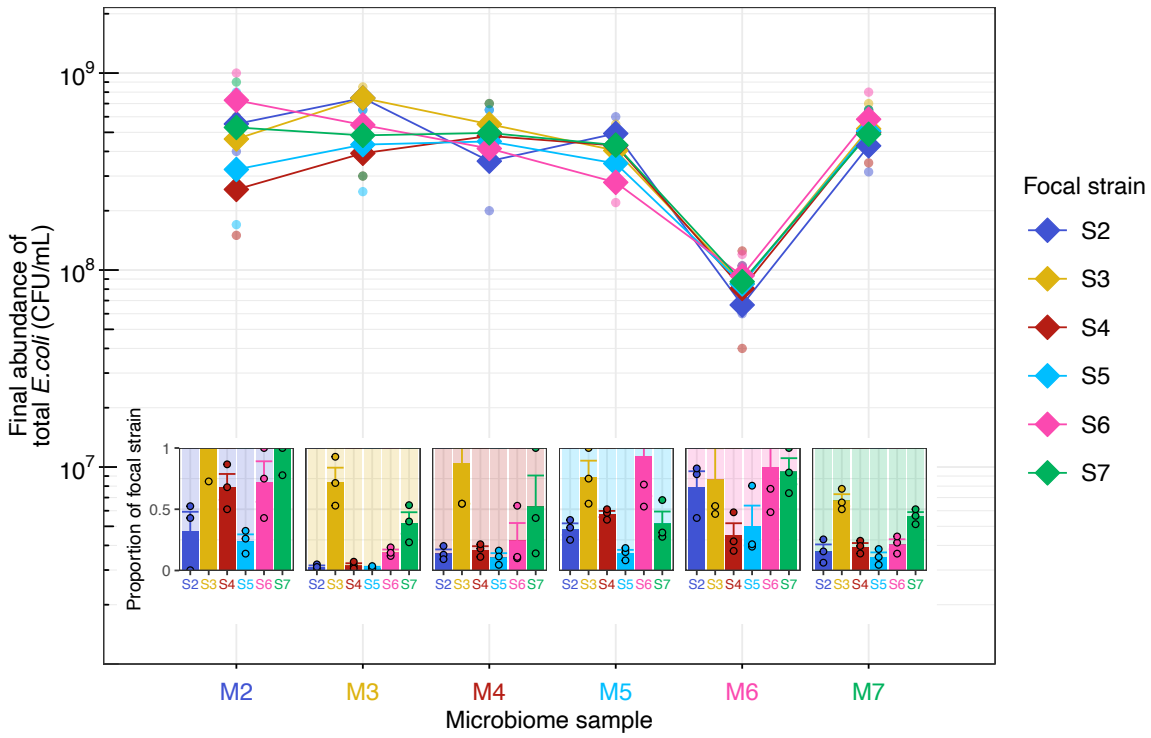

167

168 **Fig. 2: Total *E. coli* abundance and proportion contributed by focal strains in human-gut microcosms.** Main
169 panel: final abundance of total *E. coli* (including focal and resident populations) for each live microcosm (Fig. 1a),
170 estimated by plating on chromatic agar without antibiotic. Dots show individual replicates, diamonds represent
171 the average in each combination (geometric mean), and lines connect averages for each focal strain across
172 microbiome samples. Insets: proportion of total *E. coli* represented by the focal strain, obtained by dividing the
173 focal strain's absolute abundance (Fig. 1a) by the corresponding total *E. coli* abundance (main panel of this
174 figure) for each replicate. Dots show individual replicates and bars/error bars show mean/standard error for
175 each focal strain-microbiome combination. The y-axis scale is limited to 1; individual dots, bars and sections of
176 error bars above 1 due to noise of the method are not displayed. The background colors in lighter shades
177 represent the corresponding most abundant resident strain (e.g., yellow background in microbiome sample 3,
178 M3, corresponds to the original untagged strain 3, S3).

179 **Interspecific interactions involving acidification contribute to microbiome-specific finite *E. coli* abundance**

180 Aside from resident *E. coli*, differences in the composition or abundance of other resident taxa may alter
181 ecological interactions that determine the success of the incoming strains. Consistent with this possiblilty, we
182 observed substantial variation in taxonomic composition among samples prior to cultivation in microcosms
183 (Fig. 3a, Supplementary Fig. 12). In particular, microbiome sample M6 had a high proportion of Enterococcaceae
184 (27%, brown, Fig. 3a) —not detected in other samples except M4, where its relative abundance was only 0.3%—
185 and a relatively high proportion of Bacteroidaceae compared to other samples (26% vs. mean ± s.d.: 7% ± 3% in
186 other samples, lightest pink, Fig. 3a). M6 also had a relatively low abundance of resident *E. coli* prior to
187 cultivation, shown by both 16S sequencing (all reads assigned to Enterobacteriaceae were of a single amplicon
188 sequence variant, ASV, assigned to *E. coli* and made up 0.02% in M6 vs. mean ± s.d.: 0.06% ± 0.01% in other
189 samples; Supplementary Fig. 12b) and plating (Supplementary Fig. 13a). In terms of total bacterial diversity, M6
190 was less diverse than other samples (Fig. 3b). The distinctiveness of this sample was further supported by final
191 abundances after our main experiment: total bacterial abundance was approximately 50% lower in microcosms
192 produced with M6 compared with other samples (measured by flow cytometry, Fig. 3c). This trend was even
193 stronger for *E. coli*, in that final total *E. coli* abundance was approximately six-fold lower in microcosms produced
194 with M6 compared with other samples (Fig. 2, Supplementary Fig. 13b), and average focal strain performance
195 was lowest in M6 (Fig. 1a). Thus, microcosms prepared with microbiome sample M6 were the least favourable
196 for microbial growth and particularly for *E. coli*, including our focal strains.

197 We next investigated possible causes of the relatively low focal-strain abundances reached in M6
198 microcosms (Fig. 1a). This effect was not observed in sterile microcosms prepared with sample M6 (Fig. 1b),
199 suggesting that the relatively unfavorable conditions in M6-microcosms emerged during incubation of the
200 resident microbiota. The most striking feature of the M6 resident microbiota was the high abundance of
201 Enterococcaceae (three ASVs all assigned to *Enterococcus faecium*), which produces lactate during fermentation
202 of carbohydrates [40]. This observation led us to hypothesize that acidification of the microcosm environment
203 could contribute to the unfavourable growth conditions. Supporting this, the final pH of M6 microcosms was
204 considerably lower than that of microcosms prepared with other microbiome samples (on average 5.4 in M6 vs.
205 mean ± s.d. 6.1 ± 0.2 in other samples, Fig. 3d). To test for a causal relationship between low pH and reduced
206 focal-strain growth, we collected supernatant from microcosms prepared with each sample (cultivated in the
207 same conditions as the main experiment but without introducing focal strains) and assessed the growth
208 dynamics of each focal strain in these supernatants (Supplementary Figs. 14 and 15). In contrast to supernatants
209 from other samples, which were less acidic (pH>5.5), the supernatant from M6-microcosms (pH<5.5) did not
210 support any focal-strain growth (Supplementary Fig. 14, Fig. 3e, left panel). However, this growth impairment
211 was reversible: neutralizing the pH of the M6-supernatant with sodium hydroxide restored growth of all focal
212 strains (Fig. 3e, right panel). In summary, the distinctive taxonomic composition of the M6 microbiota led to
213 substantial acidification of the microcosm environment, limiting *E. coli* growth (Fig 2). This process helps to
214 explain the microbiome-to-microbiome variation observed in our main experiment (Fig. 1).

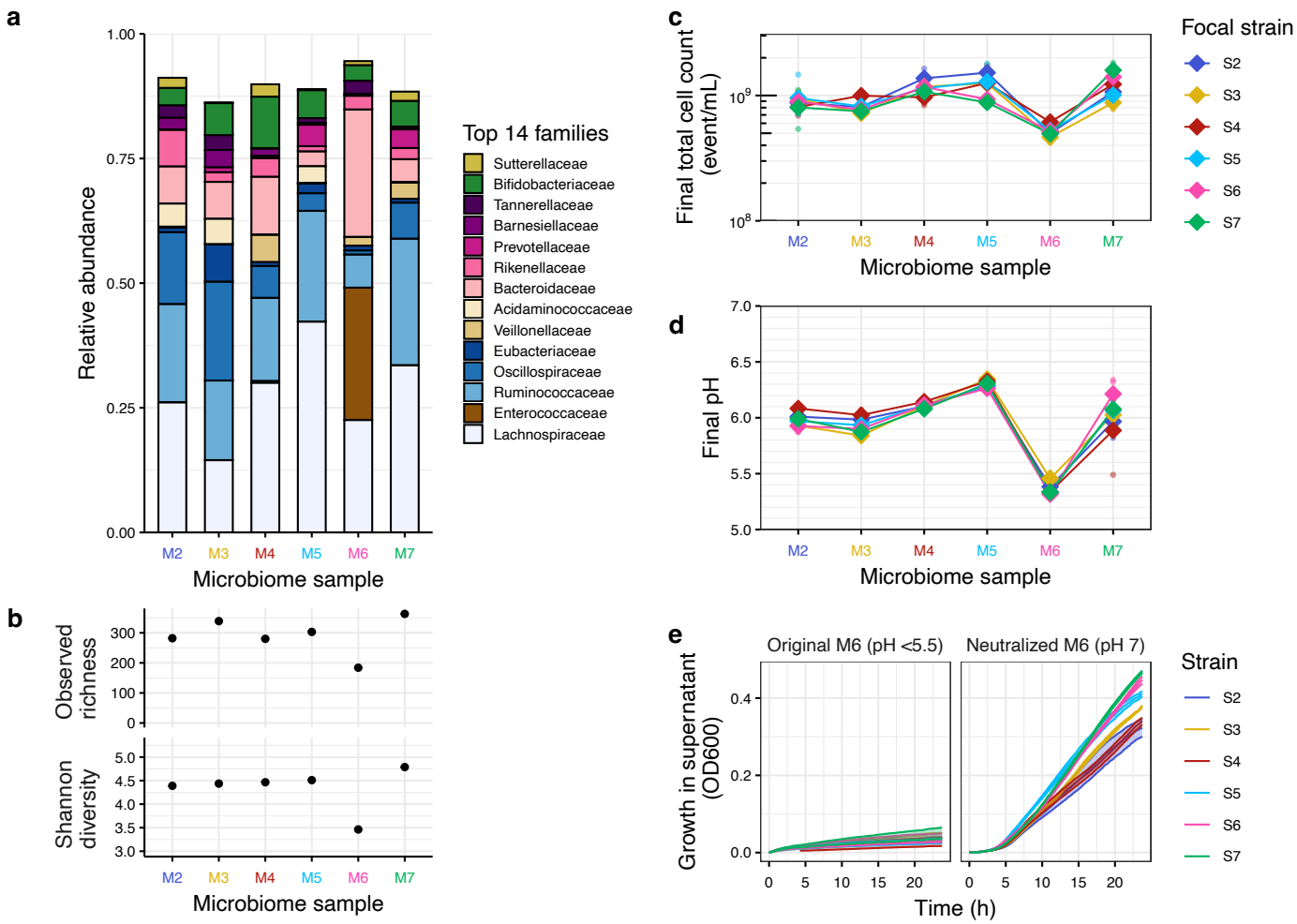

Fig. 3: Taxonomic composition and pH-mediated growth constraints. **a** Taxonomic composition of microbiota from the six samples before cultivation. Relative abundance of the fourteen most abundant families across samples, ordered and colored based on phylum (from top to bottom: Proteobacteria in yellow, Actinobacteriota in green; Bacteroidota in pink shades; and Bacillota, further distinguished by class: Negativicutes in beige shades, Bacilli in brown and Clostridia in blue shades). Within phylum, families are ordered by ascending abundance. **b** Alpha diversity (Observed richness and Shannon diversity index) based on ASV-level data for each microbiome sample before cultivation. **c** Final total cell counts in the live microcosms estimated by flow cytometry. Diamonds represent the average (geometric mean) of three replicated microcosms (points for each focal strain and microbiome sample combination) and lines connect the average outcome for microcosms prepared with a given focal strain across microbiome samples. **d** Final pH in the live microcosms. These values show a weak correlation with final abundance of focal strains (Supplementary Fig. 16, R=0.33, p=0.049), largely driven by sample M6. **e** Growth of focal strains under aerobic conditions over 24h (approximated by biomass production, i.e. optical density at 600 nm, OD_{600}) in the sterilized supernatant of cultivated microcosms (prepared with the microbiome sample M6 and incubated as in Fig. 1, but without inoculating focal strains) and in the corresponding supernatant adjusted to a neutral pH (7.0). Each curve represents the mean ± standard error of the mean (SE) of three replicates, shown as solid lines with shaded areas of the same color. Equivalent growth measurements in supernant from other microbiome samples are presented in Supplementary Figs. 14 and 15.

Transplanting a single taxon across microbiome samples predictably alters resident microbiome-level properties, including *E. coli* growth

We then sought to use the distinctive M6 microbiome as a case study to investigate how resident microbiota contribute to the observed variation of *E. coli* growth among samples from different people (Fig. 1a and 2). Screening taxa from cultivated M6 microcosms, we identified a *C. butyricum* strain that acidified the basal medium in pure culture to a degree comparable with that observed in our earlier experiments with the full M6 microbiome sample (see Methods and Supplementary Fig. 17). This species was not detected in cultivated microcosms from other microbiome samples. *C. butyricum* is a spore-forming anaerobe found in the environment and the gut of humans and animals [41]. It produces butyrate and other short-chain fatty-acids (SCFAs), and is increasingly recognized as probiotic species with documented health benefits in animal models and humans (reviewed in [41]). To test whether *C. butyricum* contributed to the reduction in total *E. coli* abundance in M6, and whether similar effects could be reproduced in different microbiome backgrounds, we transplanted the isolated strain into gut microcosms prepared with the other five samples (M2, M3, M4, M5, M7). Compared with control microcosms (prepared with the same samples but not inoculated with *C. butyricum*), addition of *C. butyricum* markedly reduced final pH of the microcosms ($F_{1,20}$=1477.9, p<0.001), reaching levels comparable to M6 (Fig. 4a). Acidification occured in four of the five tested samples (interaction term: $F_{4,20}$=175.9, p<0.001; significant negative effect for all samples except M4 by post-hoc comparisons using estimated marginal means) and was accompanied by shifts in fermentation product profiles (Fig. 4b). Across all microbiome samples, inoculation with *C. butyricum* led to substantial increases in butyrate concentration relative to control microcosms (+14.8 mM on average, t_4 = 6.28, p<0.001), and decreases in acetate and lactate concentration (acetate:–8.08 mM on average, t_4 = –4.37, p = 0.012; lactate: –6.45 mM, t_4 = –2.33, p = 0.080). Butyrate production in gut microcosms inoculated with *C. butyricum* even exceeded that of *C. butyricum* pure cultures (17.7± 5.4mM vs. 7.0 mM, Supplementary Fig. 18) and among control microcosms, butyrate production was higher in M6 microcosms than microcosms prepared with other microbiome samples (12.9 mM vs. mean ± s.d 2.5 ± 1.8mM, Supplementary Fig. 18). Collectively, these results indicate that *C. butyricum* played a key role in sample M6's functional profile, and its addition to other microbiome samples was sufficient to establish similar abiotic conditions.

We next asked whether addition of *C. butyricum* affected other bacteria. This showed transplantation of *C. butyricum* into other microbiome samples suppressed *E. coli* growth ($F_{1,20}$=117.53, p<0.001, Fig. 4c), to a variable extent depending on the sample (interaction term: $F_{4,20}$=5.45, p=0.0034; significant negative effect in M2, M4, M5 by posthoc tests). Note the most abundant resident *E. coli* strain in each sample corresponded to one of the five focal strains from the main experiment (Fig. 1). Addition of *C. butyricum* also reduced total bacterial growth on average ($F_{1,20}$=25.99, p<0.001, Fig. 4d), again with microbiome-specific effects (interaction term: $F_{4,20}$=7.39, p<0.001; significant negative effect in M2, M4, M5 by posthoc tests). Profiling of community composition with 16S rRNA sequencing revealed that taxonomic composition was also altered by addition of *C. butyricum* (Fig. 4e, PERMANOVA after removing reads attributed to *C. butyricum*, F(1,20) = 37.64, R^2 = 0.069, p = 0.001), with microbiome-specific effects (interaction term: F(4,20)= 8.04, R^2 = 0.059, p =0.001). Consistent with this, linear discriminant analysis effect size (LEfSe [42]) revealed multiple taxa that were either enriched or

271 suppressed upon *C. butyricum* supplementation, in terms of relative abundance within each microbial
272 community compared with the corresponding control microcosms and after excluding reads assigned to
273 *C. butyricum* (Fig. 4e, Supplementary Fig. 19). Some taxa were affected consistently across samples; notably the
274 lactate-producing Enterococcaceae family was suppressed, whereas the Ruminococcaceae family, including
275 some well-known butyrate producers such as *Faecalibacterium prausnitzi* [40], was enriched (Fig. 4e,
276 Supplementary Fig. 19). Other taxa exhibited variable responses depending on the microbiome background,
277 such as Lachnospiraceae and Bifidobacteriaceae. Despite a low inoculum chosen to mimic its natural abundance
278 in the original M6 microbiome (see Methods), *C. butyricum* established a substantial population in all inoculated
279 microcosms (28.9% ±11.1% of the community, Supplementary Fig. 20). Overall, these results show *C. butyricum*
280 suppressed growth of some resident bacteria, including *E. coli*, and reshaped community stucture, with some
281 effects consistent across human microbiome samples and others microbiome-specific.
282
283 **Fig. 4: Effects of *C. butyricum* transplantation in human-gut microcosms. a** Final pH of gut microcosms
284 cultivated with original microbiome samples (without addition of *C. butyricum*; round symbols, left) and the
285 same microbiome samples inoculated with *C. butyricum* (diamond symbols, right). Small points show individual
286 replicates; larger points show geometric means. Two additional controls are shown to the right of the black line:
287 the original M6 microbiome sample, in which *C. butyricum* was naturally present (pink) and microcosms
288 prepared without any microbiome sample (labelled none), but with *C. butyricum* in pure culture (grey). **b**
289 Changes in concentrations of six fermentation products in supernatants of cultivated microcosms with
290 microbiome samples inoculated with *C. butyricum* relative to equivalent microcosms without addition of *C.*
291 *butyricum* (as in (a)). Bars show differences between the two treatment averages for each compound and
292 microbiome sample. Individual replicates are shown in Supplementary Fig. 18. **c** Final *E. coli* abundance
293 (estimated by plating on chromatic agar) in gut microcosms cultivated with the original microbiome samples
294 uninoculated and the same microbiome samples inoculated with *C. butyricum* (as in (a)). **d** Final total cell counts
295 (estimated by flow cytometry) in gut microcosms cultivated with the original microbiome samples and the same
296 microbiome samples inoculated with *C. butyricum* (as in (a)). **e** Non-metric multidimensional scaling (NMDS)
297 based on Bray-Curtis distances of ASV-level abudances in cultivated gut microcosms. Reads attributed to
298 *C. butyricum* were removed prior to analysis to focus on shifts in the resident microbiota. Each point represents
299 an individual replicate, colored by microbiome and shaped by treatment (without addition of *C. butyricum*,
300 circles; inoculated *C. butyricum*, diamonds). Closed loops connect the three replicates for each microbiome-
301 treatment group (stress value=0.11). **f** LEfSe analysis performed on family-level taxonomic composition of the
302 cultivated gut microcosms, with reads attributed to *C. butyricum* removed prior to analyis. Analyses were
303 performed separately for each microbiome sample, with families aggregated from ASVs. Only families with an
304 LDA score >4 in at least one microbiome are shown. Circle size is proportional to absolute LDA score and circle
305 color indicates direction the effect (suppression or enrichment in *C. butyricum*-inoculated microcosms relative
306 to control microcosms without addition of *C. butyricum;* see legend).
307

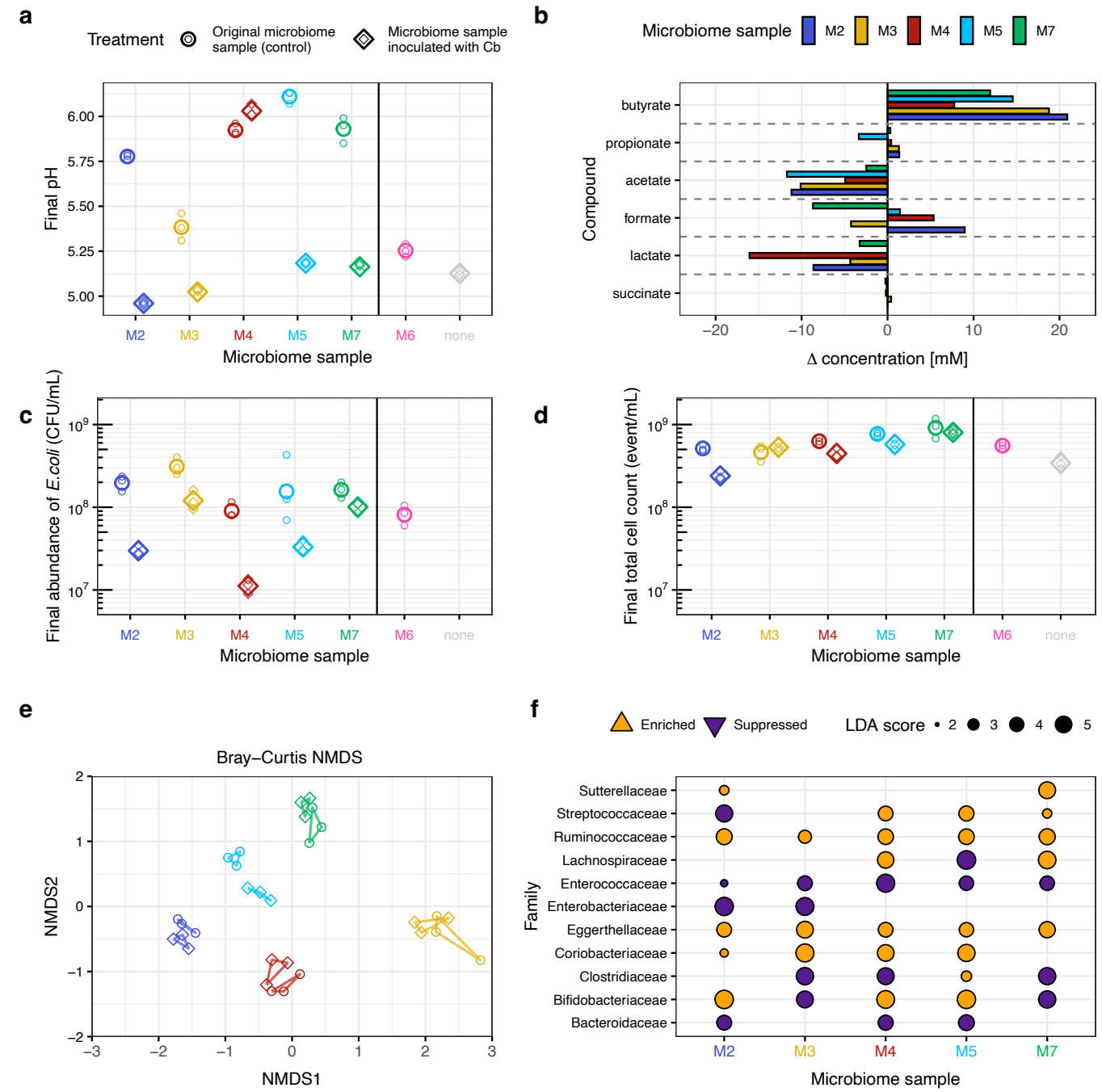
a
Treatment
Original microbiome sample (control)
Microbiome sample inoculated with Cb
Final pH
6.00
5.75
5.50
5.25
5.00
M2
M3
M4
M5
M7
M6
none
Microbiome sample
b
Microbiome sample
M2
M3
M4
M5
M7
Compound
butyrate
propionate
acetate
formate
lactate
succinate
−20
−10
0
10
20
Δ concentration [mM]
c
Final abundance of E.coli (CFU/mL)
10^9
10^8
10^7
M2
M3
M4
M5
M7
M6
none
Microbiome sample
d
Final total cell count (event/mL)
10^9
10^8
10^7
M2
M3
M4
M5
M7
M6
none
Microbiome sample
e
Bray–Curtis NMDS
NMDS2
2
1
0
−1
−2
−3
−2
−1
0
1
2
3
NMDS1
f
Enriched
Suppressed
LDA score
2
3
4
5
Family
Sutterellaceae
Streptococcaceae
Ruminococcaceae
Lachnospiraceae
Enterococcaceae
Enterobacteriaceae
Eggerthellaceae
Coriobacteriaceae
Clostridiaceae
Bifidobacteriaceae
Bacteroidaceae
M2
M3
M4
M5
M7
Microbiome sample

3

309 ## Discussion

310 Our reciprocal transplant experiment showed that both absolute and relative population growth of focal *E. coli*
311 strains varied among microbiome samples from different individuals. Intraspecific competition and the resulting
312 displacement of conspecifics shaped strain performance within microbiome samples, each with an inherent
313 finite total *E. coli* abundance. In turn, this variation in total *E. coli* abundance among samples was explained by
314 interspecific interactions involving acidification. We identified a strain of *C. butyricum* contributing to this effect
315 and showed that its transplantation into other microbiome samples reproducibly alters abiotic conditions and
316 biotic interactions.

317 An important implication of our results is that average growth of commensal *E. coli* varies among
318 samples from different people, with acidification emerging as one driver of this variation. This suggests inter-
319 individual microbiome variation is a key driver of susceptibility to colonisation by incoming *E. coli* and its relative
320 abundance compared to other taxa. This matters because, although individuality in terms of taxonomic
321 composition of human microbiomes is widely documented [8,43], the functional consequences of this are less
322 understood, aside from evidence that dysbiosis can promote colonization by pathogens such as *Clostridioides*
323 *difficile* [44]. Here, we demonstrate that an even more common form of microbiome variation, among samples
324 from healthy individuals, also has functional consequences. In sample M6, resident microbes acidified the local
325 environment below pH 5.5, largely overcoming the buffering capacity of the basal medium, and inhibiting *E. coli*
326 growth. Microbially driven acidification and its downstream impacts on the growth of other taxa are common in
327 natural microbial communities [45], including in the gut, where some taxa contribute to mild acidification (pH
328 5.5-6), while others, including *E. coli*, thrive under close-to-neutral conditions (pH 6.5-7) [46,47]. The extent and
329 dynamics of acidification probably differ among individual microbiomes, due to physiological and dietary
330 differences [48], and between spatially and temporally heterogeneous natural settings and our microcosm
331 system. Nevertheless, our findings suggest acidification may be a common mechanism by which person-to-
332 person microbiome variation translates to variable colonization outcomes.

333 A second implication of our findings is that average *E. coli* growth in a given microbiome can be strongly
334 influenced by a single taxon. Though our study was not designed to explicitly test the link between diversity and
335 colonization resistance, microbiome sample M6 had the lowest diversity among our samples (Fig. 3b), yet
336 showed the stongest suppression of incoming *E. coli* strains, an effect we reproduced by transplanting
337 *C. butyricum* into other microbiome samples. This indicates that functional features, rather than diversity per
338 se, can be decisive in determining colonization outcomes. In turn, this has potentially promising implications in
339 the context of microbiota-oriented health interventions. *C. butyricum* has already emerged as a next-generation
340 probiotic [49,50], with strains such as MIYAIRI 588 used in Asia for decades. However, the ecology of this species
341 remains incompletely characterized. Our results provide new insights in this context in three ways. First, the
342 *C. butyricum* strain we isolated was naturally circulating and identified serendipitously upon microbiome
343 screening, suggesting such interspecies interactions can occur inherently and contribute to inter-microbiome
344 differences even without probiotic intervention. Second, these interactions would remain invisible in
345 sequencing-based surveys. Consistent with this, a recent metagenomic survey of natural Enterobacteriaceae co-
346 excluder taxa [27] did not identify *C. butyricum* among these taxa, despite detecting an overall enrichment in

347 metabolic gene clusters involved in SCFA production. This could reflect both the typically low abundance of this
348 taxon (no ASV assigned to Clostridiaceae in our sample prior to cultivation) and its relatively low prevalence
349 across individuals [51], underscoring how functional consequences of individual-specific taxonomic composition
350 may be missed in sequencing-based analyses. Meanwhile, our microcosm set-up allowed us to detect the
351 functional impact of this species upon cultivation, but it may fail to detect interactions mediated by more
352 fastidious taxa. Third, our replicated and controlled microcosm approach enabled us isolate *C. butyricum's*
353 impact on other microbes in healthy-human samples, which is not readily disentangled in animal models [52–
354 54] and human intervention studies [55,56]. This revealed increased butyrate production and suppression of
355 taxa such as Enterobacteriaceae and Enterococcaceae, pointing to a role in colonization resistance [57,58].

356 A further key finding is that, within microbiome-specific finite *E. coli* abundance, the relative
357 performance of strains varied among samples, while the strain rank order remained generally consistent. This
358 consistency of rank order, resulting in a lack of detectable signature of local adaptation, advances our
359 understanding of the extent to which strains are matched to individual microbiomes. Our results are inconsistent
360 with the idea that the most abundant resident *E. coli* strain from a given microbiome performs relatively well in
361 that microbiome compared to 'foreign' strains, or that the home microbiome of a given strain is relatively
362 favourable for that strain compared to other microbiomes. We do not exclude that stronger signatures of local
363 adaptation may be found in other species, such as strict anaerobes with more limited dispersal than aerotolerant
364 microorganisms [59]. Future work expanding tests for local adaptation in human-associated microbiomes may
365 reveal pattern similar to those observed in other ecosystems, where signatures of local adaptation are
366 sometimes detected [23–25] and sometimes not [21,22].

367 Our results provide new information about the ecological processes driving competition among *E. coli*
368 strains in human-associated microbial communities. Previous work with mice and synthetic communities
369 suggests that incoming strains are suppressed if resident microbes block access to nutrient niches [10,60]. In our
370 system with microbial communities sampled directly from humans and thereby accounting for some interactions
371 and complexity not captured by other approaches, we found no positive association between incoming strain's
372 ecological success and its metabolic profile relative to the most common resident conspecific (Supplementary
373 Fig. 7). While nutrient competition may play a central role in other experimental conditions with defined limiting
374 nutrients, our results suggest that other mechanisms may have a stronger influence over strain-level *E. coli*
375 success in complex human-associated communities. One such mechanism is direct antagonism mediated by
376 colicin production. Successful strains produced colicin E1, achieving detectable inhibition of some competitors.
377 However, acquiring the plasmid and the corresponding inhibitory phenotype did not boost ecological success of
378 another strain in live microcosms (Supplementary Fig. 10). This does not rule out colicin E1 contributing to the
379 ecological success of strains S3 and S7, but highlights the need to investigate the conditions in which colicins are
380 deployed by *E. coli* populations of different genetic background competing in the gut.

381 Finally, our results open up new questions about the impact of *E. coli* population structure on
382 colonization success of different gut microbiome samples by individual strains. For example, it is possible that in
383 nature some variability of ecological performance among strains is linked to their phylogenetic relatedness, with
384 more closely related strains potentially sharing some phenotypes [61]. Our results are in some ways consistent

with such a trend, in that the two relatively successful strains S3 and S7 belong to the same phylogroup and share some phenotypes (metabolic profile and direct inhibition). However, we would need a much larger number of strains to properly assess the role of phylogenetic structure in colonisation of human samples. Furthermore, although working with samples from different people allowed us to investigate drivers of ecological success among independent human-associated microbial communities, a different experimental design and scale would be needed to quantify the contribution of the identity of the donor to the observed sample-to-sample variation. To do this, more than one sample per individual would be required and, ideally, metadata to allow associations with host factors such as age, diet or immune status to be tested.

In conclusion, our study shows that natural variation in the human gut microbiome has functional consequences, shaping ecological interactions and the success of incoming bacterial strains. While this variation complicates predictions of colonization outcomes, we identified a transferable interspecies interaction that controls *E. coli* growth. These findings improve our understanding of how resident microbes shape colonization outcomes and provide a foundation for microbiome-targeted interventions.

398 # Material and methods

399 **Human microbiome samples**

400 Stool samples were collected at the Department of Environmental Systems Science of ETHZ on the 17th of March
401 and the 24th of Mai 2022 from anonymous above-18-year-old healthy donors, who had a body mass index
402 between 19 and 25, were not recovering from surgery, had not taken antibiotics in the previous six months, and
403 did not test positive for SARS-CoV-2 in the previous two months. The sampling protocol was approved by the
404 ETHZ Ethics Commission (EK 2020-N-150). Each volunteer provided one stool sample in a sealed box supplied
405 with an AnaeroGen 2.5L sachet (Thermo Scientific) to maintain an anaerobic atmosphere. We processed the
406 samples within six hours under anaerobic conditions in a vinyl chamber (Coy Labs, USA), containing 2.5 % H_2, 5%
407 CO_2 and N_2 for the rest. We resuspended stool samples 10% *w*:*v* ratio in peptone wash, prepared as previously
408 described (the following components in water, in g per liter: 1.0 peptone from casein, 0.5 L-cysteine, 0.5 bile
409 salts and 0.001 resazurin) [39]. We then froze the resulting fecal microbiome samples with 10% glycerol and
410 stored them at -80°C. For this project, we selected a subset of six fecal microbiome samples, which include a
411 resident microbiota and abiotic components [15] and are referred to as 'microbiome samples' hereafter.
412 Because we were unable to isolate *E. coli* from one sample (M1), we excluded it and replaced it with another
413 (M7). Consequently, we performed all experiments with microbiome samples M2-M7. This project developed in
414 parallel in the same laboratory with the project described in Leon-Sampedro et al. [62], which addressed
415 different questions with clinical antibiotic-resistant strains. We used the same sample collection, and
416 microbiome samples M2, M3, M4 in this study correspond to Donor1, 2, 3 in that work.

417 For 16S rRNA gene sequencing, we sent 2 mL aliquots from each sample to Microsynth AG, Switzerland,
418 for DNA extraction, amplification of the V3V4 region of the 16S rRNA gene using primers 341F
419 (5'-CCTACGGGNGGCWGCAG-3') and 805R (5'-GACTACHVGGGTATCTAATCC-3') [63], and sequencing on an
420 Illumina MiSeq instrument. We analyzed the data in R, using the package DADA2 v. 3.18 [64]. Following the
421 workflow described in [65], we filtered and trimmed reads and inferred amplicon sequence variants (ASVs)
422 against the SILVA nr.99 v.138 dataset. After filtering, we obtained a total of 81'503 ± 10'037 (mean ± s.d.) reads
423 assigned to ASVs per sample. We imported the obtained ASV table and corresponding taxa table into
424 phyloseq v 1.46 for downstream analyses and visualizations. We quantified alpha diversity using the function
425 *plot_richness* (measures=*Observed*, *Shannon*).

426

427 **Focal *E. coli* strains**

428 To isolate the focal *E. coli* strains from the samples, we plated fecal microbiome samples at several dilutions on
429 chromatic Mueller-Hinton (MH) agar (Liofilchem, Roseto degli Abruzzi, Italy). From each sample, we chose
430 randomly one purple colony, inoculated it in lysogeny broth (LB, Sigma-Aldrich) and added 25 % glycerol for
431 preservation at -80 °C. We confirmed that picked colonies were *E. coli* by amplifying and sequencing a fragment
432 of *dnaJ,* using DN1-1F (5'-GATYTRCGHTAYAACATGGA-3') and DN1-2R (5'-TTCACRCCRTYDAAGAARC-3') as
433 primers [66]. Because multiple *E. coli* strains can co-exist in the same microbiota [7,67], we tested whether the
434 picked colony isolates represented the most abundant *E. coli* strain in each sample by repetitive element
435 palindromic PCR (rep-PCR), using primers REP1R (5'-NNNGCGCCGNCATCAGGC-3') and REP2R

436 (5'-ACGTCTTATCAGGCCTAC-3') [68]. This approach allowed us to establish the fingerprint (corresponding to a
437 band pattern on electrophoresis gel) characteristic of each of the six isolated *E. coli* clones and compare it to
438 that of nine other random colonies from each corresponding sample. In five cases, the isolated *E. coli* clone
439 showed a fingerprint matching with 9/9 other colonies from the same sample, and in one case (sample M6) it
440 matched with 8/9 other colonies, indicating that in each sample, the isolated clone represented the most
441 abundant *E. coli* resident strain.

442 To be able to track these six focal strains (S2-S7) upon inoculation into gut microcosms, where there is
443 a resident microbiota including other *E. coli* cells, we tagged each of them with a selective marker. We did this
444 by electroporating the non-mobilizable plasmid pACYC184 (New England Biolabs), which encodes
445 chloramphenicol resistance [69,70]. Comparing final abundance of each focal strain in sterile microcosms
446 assessed by plating on agar with and without antibiotics (see below) indicated that the plasmid was stable in our
447 experimental conditions (based on pairwise t-tests, abundance differed in only 2/36 combinations, and in
448 different directions: M2, S3 $t(2) = -8.00$, $p=0.015$ and M3, S7 $t(2) = 5.64$, $p=0.030$, but both p-values were >0.05
449 upon adjustment for multiple testing with Bonferroni correction). Furthermore, comparing growth dynamics
450 and competitive fitness of original untagged strains vs. their tagged counterparts in basal medium
451 (Supplementary Fig. 4a and Supplementary Fig. 5b respectively) revealed a small cost of bearing the plasmid,
452 which was comparable among strains and therefore unlikely to confound other causes of strain-to-strain
453 variability in our main microcosm experiments.

454 We sequenced the whole genome of both the original untagged and the tagged version of the focal
455 strains (Supplementary Methods section **Whole-genome sequencing and analyses**). We also characterized the
456 strains phenotypically, by measuring their metabolic capacity across 96 single-carbon-source environments and
457 testing their inhibitory activity (Supplementary Methods sections **Metabolic profiling across single-carbon-**
458 **source environments** and **Agar inhibition assays**, respectively). Upon identification of the colicin E1 plasmid as
459 a putative mediator of inhibition, we transferred the plasmid by conjugation to a susceptible strain, to confirm
460 its role in mediating antagonism and test for performance of the resulting transconjugant relative to the original
461 strain in gut microcosms (Supplementary Methods).

462

463 **Anaerobic gut microcosms**

464 We quantified growth performance of the focal strains (S2-S7) among microbiome samples (M2-M7) by
465 cultivating them in anaerobic microcosms. We prepared anaerobic 8mL-microcosms in 15mL screw-cap tubes
466 (Sarstedt), containing 0.5 mL microbiome sample (either thawed, or thawed and sterilized by autoclaving for the
467 sterile-microcosms experiment) and 7.5 mL of basal medium, prepared as previously described (resuspending
468 the following components in water, in g per liter: 2.0 peptone from casein; 2.0 tryptone, 2.0 yeast extract, 0.1
469 NaCl, 0.04 K_2HPO_4, 0.04 KH_2PO_4, 0.01 $MgSO_4x7H_2O$, 0.01 $CaCl_2x6H_2O$, 2 $NaHCO_3$, 1.8 Tween 80, 0.005 hemin, 0.5
470 L-cysteine, 0.5 bile salts, 2 starch, 1.5 casein, 0.001 resazurin; adjusting the pH to 7; autoclaving and finally adding
471 0.001 g per liter menadion) [39]. We made three replicate microcosms in each combination of focal strain and
472 microbiome sample, giving 108 microcosms in total for the live- and sterile-microcosm experiments. We added
473 focal strains (tagged versions) after diluting independent overnight cultures (incubated at 37 °C statically and

474 anaerobically in 200 µl basal medium), aiming to achieve an inoculum density between 10^4 and 10^5 CFU/mL. We
475 chose this inoculum density to start with comparable amounts of focal and resident *E. coli* (Supplementary Fig.
476 13a). We incubated microcosms at 37 °C, statically and anaerobically for 24 h. This single 24-h growth cycle was
477 selected based on our previous findings [39], which showed that this timeframe captures variation in focal strain
478 population growth while maintaining the dominant family-level structure of the original inoculum. Although
479 fast-growing facultative anaerobes (particularly Enterobacteriaceae and Enterococcaceae) are predictably
480 enriched under these conditions [71], the short cultivation period preserves ecologically relevant community
481 interactions.

482 We assessed abundance of focal strain and total *E. coli* by sampling 200 µl from well-mixed microcosms
483 and spot-plating dilutions on chromatic MH agar plates supplemented with 25 µg/mL chloramphenicol and
484 without antibiotics respectively. For all microcosm experiments, we supplemented aliquots or the whole volume
485 of the cultivated microcosms with 10% glycerol and stored them at -80 °C for further use.

486 In live microcosms, effective starting densities varied among focal strains ($F_{5,72}$=52.85, p<0.001, ranging
487 between 2×10^4 and 8×10^5 CFU/mL, Supplementary Fig. 21a). A separate experiment, in which we inoculated
488 one focal strain at different densities into three different microbiome samples, indicated that within this range,
489 final abundance was independent of inoculum density (R=0.23, p=0.25, Supplementary Fig. 21b). Therefore, we
490 took final abundance as a measure of focal strain growth performance. For statistical analysis, we applied
491 analysis of variance (ANOVA, aov in R) with strain, microbiome, and their interaction as factors, and log-
492 transformed CFU counts as the response variable. For both live- and sterile-microcosm experiments, we
493 quantified average local adaptation, defined as the sympatric-allopatric contrast [17] (Supplementary Methods
494 section **Quantifying local adaptation**).

495 We estimated total bacterial abundance in aliquots from live microcosms from the main experiment
496 using flow-cytometry. We thawed aliquots of the 108 microcosms, diluted them 1:1000 in 200 µl phosphate-
497 buffered-saline (PBS) and stained cells with the addition of SYBR Green (Invitrogen, Thermo F. Scientific). We
498 used a Novocyte 2000R (ACEA Biosciences, San Diego, CA, USA) with the following parameters: 50 µl flow rate,
499 14.6 core diameter and 100'000 events recorded per sample. We measured pH in supernatant from the 108
500 microcosms from the main experiment, after thawing and centrifuging them, using a portable pH-meter FiveGo
501 F2 (Mettler Toledo).

502 In a separate experiment, we estimated initial and final abundance of resident *E. coli* in the absence of
503 tagged focal strains (Supplementary Fig. 13), preparing and cultivating microcosms in the same way as we did
504 for the live microcosm experiment, but without inoculating focal strains. Here as well, we made three parallel
505 replicates, giving a total of 18 microcosms. We made pH measurements by thawing the 18 cultivated microcosms
506 and using the pH-Fix 2.0-9.0 test-strips (Macherey-Nagel). From the same microcosms we prepared supernatant,
507 removing bacterial cells by centrifugation (4000 g, 10 min) and sterile filtering with a pore size 0.2 µm (Filtropur
508 S, Starstedt). We adjusted the pH of each supernatant by adding few microliters of 1M sodium hydroxide and
509 remeasuring, until reaching a pH of 6.5-7 (up to 6 mM sodium hydroxide in the three supernatants from M6
510 microcosms).
511

512 **Growth dynamics of focal strains**

513 We monitored population growth dynamics of each focal strain in various conditions (basal medium, sterile
514 microcosm conditions and supernatant of cultivated microcosms) and always aerobically. To do so, we diluted
515 independent overnight cultures (incubated at 37 °C shaking and aerobically in 200 µl basal medium) 1:1'000 in
516 200 µl of the corresponding media in a microplate. We then incubated microplates at 37 °C in a plate reader
517 (Tecan NanoQuant Infinite M200 Pro), shaking and measuring optical density at 600 nm (OD600) every 15 min
518 and during 24 h. To assess contribution of strain identity and selective marker (pACYC184) to the variability of
519 growth dynamics, we monitored growth of both tagged and untagged version of each focal strain in basal
520 medium (Supplementary Fig. 4a). In all other conditions, we characterized growth of the tagged version of focal
521 strains exclusively. To monitor growth in sterile microcosm conditions (Supplementary Fig. 4b and
522 Supplementary Fig. 14), we prepared one tube per sample containing 0.5 mL of autoclaved microbiome sample
523 and 7.5 mL of basal medium, and we let particles sediment overnight at 4 °C. We then inoculated each focal
524 strain in each sterile microcosm medium, with three replicates for each strain-microbiome combination. To
525 monitor growth across supernatants of cultivated microcosms (Fig. 3e, Supplementary Fig. 14), we inoculated
526 each focal strain into three replicated supernatants from each microbiome sample, prepared as described
527 above.

528 To estimate focal strains' fitness in different conditions, we estimated maximal growth rates and area
529 under the curve from all pure culture growth curves and to quantify relative competitive fitness we performed
530 a pairwise competition experiment in basal medium (Supplementary Methods section **Quantifying absolute and**
531 **relative competitive fitness of focal strains**).

532

533 ***C. butyricum* isolation and supplementation experiment**

534 We plated several dilutions of cultivated microcosms on TPY broth agar (Condolab) under anaerobic conditions
535 and incubated them for 40h. We inspected colony morphology on plates from M6 microcosms and picked all
536 colonies with a visibly distinct morphology. We submitted those isolates to MALDI-TOF analysis and detected
537 four distinct species: *E. coli*, *E. faecium*, *Bifidobacterium longum* and *C. butyricum*. We subsequently cultured
538 each isolate in basal medium and measured pH of the cultures at an endpoint with pH-meter FiveGo F2. We
539 found that only the *C. butyricum* acidified basal medium (Supplementary Fig. 17). We stored some sterile
540 supernatant of all replicates of these cultures at 4 °C . We inspected plates from other samples looking for
541 colonies with the characteristic morphology of *C. butyricum* (slightly irregular shape, creamy and notably larger
542 than *E. coli* colonies) but did not detect any. We also revisited the 16S rRNA data from the microbiome samples
543 to query ASVs assigned to the Clostridiaceae family. None were detected in sample M6 and only a small number
544 of reads were assigned to an unknown species within the *Clostridium sensu stricto 1* genus in some other
545 samples (27 reads in M2, 48 in M3, and 10 in M5). We concluded that in sample M6, *C. butyricum* accounted for
546 fewer than 10^4 CFU/mL (as it was represented by less than one read per 100'000, within a total bacterial load of
547 approximatively 10^9 CFU/mL).

548 We performed a supplementation experiment in gut microcosms by preparing triplicate 8-mL anaerobic
549 cultures in basal medium from five microbiome samples (M2, M3, M4, M5 and M7) as described above. For each

550 sample, cultures were either supplemented with *C. butyricum* or left untreated as controls. In addition, we
551 included triplicates of the original microbiome sample M6 as a reference, giving 33 microcosms in total, as well
552 as pure *C. butyricum* cultures. Supplementation was performed by inoculating *C. butyricum* independent
553 overnight cultures diluted 1:1'000. We incubated microcosms for 24 h and estimated *E. coli* abundance by plating
554 on chromatic agar and total bacterial abundance with flow cytometry as described above. We also measured pH
555 and stored sterile filtered supernatants at 4 °C for further characterization. For statistical analysis, we applied
556 analysis of variance (ANOVA, aov in R) with treatment, microbiome, and their interaction as factors, and log-
557 transformed CFU counts as the response variable. We used the emmeans package to compute estimated
558 marginal means and performed pairwise comparisons of treatments within each microbiome.
559
560 **Fermentation products and taxonomic profiling of cultivated microcosms**
561 We quantified six key fermentation products (succinate, lactate, formate, acetate, propionate, and butyrate) in
562 culture supernatants of the 33 cultivated microcosms and pure cultures using high-performance liquid
563 chromatography (HPLC). We injected 20 µL of each sample into a Phenomenex Rezex ROA–Organic Acid H^+ (8%)
564 column at 40 °C, using 2.5 mM H_2SO_4 in water as the mobile phase with a flow rate of 0.4 mL min^{-1}, as described
565 in [72]. To prepare calibration curves and define the expected retention times, we injected metabolite mixtures
566 with each metabolite at concentrations of 1, 5, 10, 15, and 20 mM (sodium salts, Sigma-Aldrich). For each
567 standard and sample, the refractive index detector recorded signals over 40 min, and we exported
568 chromatographic data as detector response (µRIU) versus time (s). We processed the data in Python using SciPy.
569 Implementing the workflow outlined in hplc-py [73], we applied baseline correction (*minimum_filter1d*),
570 detected peaks (*find_peaks*), and fitted multi-Gaussian models (*curve_fit*) accounting for both expected and
571 unexpected peaks. We verified peak fitting accuracy by generating diagnostic plots with Matplotlib. Finally, we
572 integrated peak areas and converted the areas into concentrations using the calibration curves.
573 We profiled taxonomic composition of the 33 cultivated microcosms from the *C. butyricum*
574 supplementation experiment with 16S rRNA sequencing using the same workflow as for the fecal microbiome
575 samples (see above). Quality control and filtering resulted in 107'836 ± 9339 (mean ± s.d.) reads assigned to
576 ASVs per sample. We used the phyloseq framework in R to aggregate ASVs to family level and summarize
577 community composition with relative abundance barplots (Supplementary Fig. 20). For downstream analyses,
578 we excluded sample M6 and removed reads attributed to *C. butyricum*. We assessed beta diversity using the
579 ASV abundance matrix and performed ordination via non-metric multidimensional scaling (NMDS)
580 with *metaMDS* from the vegan package (v. 2.7-1), specifying Bray–Curtis dissimilarities (distance=*bray*). We
581 visualized differences in microbial communities across treatments and microbiomes with NMDS plots. We tested
582 the effects of treatment and microbiome on community composition using PERMANOVA via the
583 *adonis2* function applied to Bray–Curtis distances. We assessed differential abundance of taxa across
584 treatments using *lefser* from the microbiomeMarker package (v.1.8.0). We performed analyses at different
585 taxonomic levels (Family and Genus) within each microbiome sample separately, identifying taxa with significant
586 LDA scores as enriched or suppressed in response to treatment. Finally, we combined results from all samples
587 for visualization.

Data availability

Sequences of the genomes of the six *E. coli* strains and 16S rRNA amplicons from the six fecal microbiome samples and from the 33 cultivated microcosms are uploaded to ENA (European Nucleotide Archive) and accessible through project PRJEB80311. The code and all other data supporting the findings of this study will be made available on Figshare (https://doi.org/10.6084/m9.figshare.27854763) upon publication.

Acknowledgements

We thank the Pathogen Ecology group, Carolin Wendling and Angus Buckling for their feedback. We thank the team at the Clinic for Infectious Diseases and Hospital Epidemiology of the University Hospital Zurich (USZ) for providing access to MALDI-TOF and for their support.

Funding: Swiss National Science Foundation project 310030_192428.

Declaration of interests

The authors declare no competing interests.

603 # References

604 1. Dominguez-Bello MG, Costello EK, Contreras M *et al.* Delivery mode shapes the acquisition and structure of
605 the initial microbiota across multiple body habitats in newborns. *Proceedings of the National Academy of*
606 *Sciences* 2010;**107**:11971–5.

607 2. Bokulich NA, Chung J, Battaglia T *et al.* Antibiotics, birth mode, and diet shape microbiome maturation during
608 early life. *Sci Transl Med* 2016;**8**:343ra82.

609 3. Vandeputte D, De Commer L, Tito RY *et al.* Temporal variability in quantitative human gut microbiome profiles
610 and implications for clinical research. *Nat Commun* 2021;**12**:6740.

611 4. Faith JJ, Guruge JL, Charbonneau M *et al.* The Long-Term Stability of the Human Gut Microbiota. *Science*
612 2013;**341**:1237439.

613 5. Garud NR, Pollard KS. Population Genetics in the Human Microbiome. *Trends in Genetics* 2020;**36**:53–67.

614 6. Martinson JNV, Walk ST. Escherichia coli residency in the gut of healthy human adults. *EcoSal Plus*
615 2020;**9**:10.1128/ecosalplus.ESP-0003–2020.

616 7. Martinson JNV, Pinkham NV, Peters GW *et al.* Rethinking gut microbiome residency and the
617 Enterobacteriaceae in healthy human adults. *ISME J* 2019;**13**:2306–18.

618 8. Schloissnig S, Arumugam M, Sunagawa S *et al.* Genomic variation landscape of the human gut microbiome.
619 *Nature* 2013;**493**:45–50.

620 9. Falony G, Joossens M, Vieira-Silva S *et al.* Population-level analysis of gut microbiome variation. *Science*
621 2016;**352**:560–4.

622 10. Spragge F, Bakkeren E, Jahn MT *et al.* Microbiome diversity protects against pathogens by nutrient blocking.
623 *Science* 2023;**382**:eadj3502.

624 11. Rakoff-Nahoum S, Foster KR, Comstock LE. The evolution of cooperation within the gut microbiota. *Nature*
625 2016;**533**:255–9.

626 12. Granato ET, Meiller-Legrand TA, Foster KR. The Evolution and Ecology of Bacterial Warfare. *Curr Biol*
627 2019;**29**:R521–37.

628 13. Frazão N, Konrad A, Amicone M *et al.* Two modes of evolution shape bacterial strain diversity in the
629 mammalian gut for thousands of generations. *Nat Commun* 2022;**13**:5604.

630 14. Maltby R, Leatham-Jensen MP, Gibson T *et al.* Nutritional Basis for Colonization Resistance by Human
631 Commensal Escherichia coli Strains HS and Nissle 1917 against E. coli O157:H7 in the Mouse Intestine. *PLOS ONE*
632 2013;**8**:e53957.

633 15. Marchesi JR, Ravel J. The vocabulary of microbiome research: a proposal. *Microbiome* 2015;**3**:31.

634 16. Kawecki TJ, Ebert D. Conceptual issues in local adaptation. *Ecology Letters* 2004;**7**:1225–41.

635 17. Blanquart F, Kaltz O, Nuismer SL *et al.* A practical guide to measuring local adaptation. *Ecology Letters*
636 2013;**16**:1195–205.

637 18. Leimu R, Fischer M. A Meta-Analysis of Local Adaptation in Plants. *PLOS ONE* 2008;**3**:e4010.

638 19. Hawthorne DJ, Via S. Genetic linkage of ecological specialization and reproductive isolation in pea aphids.
639 *Nature* 2001;**412**:904–7.

640 20. Marková S, Lanier HC, Escalante MA *et al.* Local adaptation and future climate vulnerability in a wild rodent.
641 *Nat Commun* 2023;**14**:7840.

642 21. Butaitė E, Kramer J, Kümmerli R. Local adaptation, geographical distance and phylogenetic relatedness:
643 Assessing the drivers of siderophore-mediated social interactions in natural bacterial communities. *Journal of*
644 *Evolutionary Biology* 2021;**34**:1266–78.

645 22. Kraemer SA, Kassen R. Patterns of local adaptation in space and time among soil bacteria. *Am Nat*
646 2015;**185**:317–31.

647 23. Scanlan PD, Hall AR, Buckling A. Parasite genetic distance and local adaptation in co-evolving bacteria–
648 bacteriophage populations. *Molecular Ecology* 2017;**26**:1747–55.

649 24. Koskella B, Thompson JN, Preston GM *et al.* Local biotic environment shapes the spatial scale of
650 bacteriophage adaptation to bacteria. *Am Nat* 2011;**177**:440–51.

651 25. Vos M, Birkett PJ, Birch E *et al.* Local Adaptation of Bacteriophages to Their Bacterial Hosts in Soil. *Science*
652 2009;**325**:833–833.

653 26. Tenaillon O, Skurnik D, Picard B *et al.* The population genetics of commensal Escherichia coli. *Nat Rev*
654 *Microbiol* 2010;**8**:207–17.

655 27. Yin Q, da Silva AC, Zorrilla F *et al.* Ecological dynamics of Enterobacteriaceae in the human gut microbiome
656 across global populations. *Nat Microbiol* 2025;**10**:541–53.

657 28. Suez J, Zmora N, Segal E *et al.* The pros, cons, and many unknowns of probiotics. *Nat Med* 2019;**25**:716–29.

658 29. Schmidt TSB, Li SS, Maistrenko OM *et al.* Drivers and determinants of strain dynamics following fecal
659 microbiota transplantation. *Nat Med* 2022;**28**:1902–12.

660 30. Buffie CG, Bucci V, Stein RR *et al.* Precision microbiome reconstitution restores bile acid mediated resistance
661 to Clostridium difficile. *Nature* 2015;**517**:205–8.

662 31. Zmora N, Zeevi D, Korem T *et al.* Taking it Personally: Personalized Utilization of the Human Microbiome in
663 Health and Disease. *Cell Host & Microbe* 2016;**19**:12–20.

664 32. Carlström CI, Field CM, Bortfeld-Miller M *et al.* Synthetic microbiota reveal priority effects and keystone
665 strains in the Arabidopsis phyllosphere. *Nat Ecol Evol* 2019;**3**:1445–54.

666 33. Brochet S, Quinn A, Mars RA *et al.* Niche partitioning facilitates coexistence of closely related honey bee gut
667 bacteria. Xavier KB, Rutz C, Xavier KB (eds.). *eLife* 2021;**10**:e68583.

668 34. Weiss AS, Burrichter AG, Durai Raj AC *et al.* In vitro interaction network of a synthetic gut bacterial
669 community. *ISME J* 2022;**16**:1095–109.

670 35. Weiss AS, Niedermeier LS, von Strempel A *et al.* Nutritional and host environments determine community
671 ecology and keystone species in a synthetic gut bacterial community. *Nat Commun* 2023;**14**:4780.

36. Barroso-Batista J, Sousa A, Lourenço M *et al.* The First Steps of Adaptation of Escherichia coli to the Gut Are Dominated by Soft Sweeps. *PLOS Genetics* 2014;**10**:e1004182.

37. Nguyen TLA, Vieira-Silva S, Liston A *et al.* How informative is the mouse for human gut microbiota research? *Dis Model Mech* 2015;**8**:1–16.

38. Barreto HC, Gordo I. Intrahost evolution of the gut microbiota. *Nat Rev Microbiol* 2023;**21**:590–603.

39. Baumgartner M, Bayer F, Pfrunder-Cardozo KR *et al.* Resident microbial communities inhibit growth and antibiotic-resistance evolution of Escherichia coli in human gut microbiome samples. *PLOS Biology* 2020;**18**:e3000465.

40. Wang SP, Rubio LA, Duncan SH *et al.* Pivotal Roles for pH, Lactate, and Lactate-Utilizing Bacteria in the Stability of a Human Colonic Microbial Ecosystem. *mSystems* 2020;**5**:e00645-20.

41. Stoeva MK, Garcia-So J, Justice N *et al.* Butyrate-producing human gut symbiont, Clostridium butyricum, and its role in health and disease. *Gut Microbes* **13**:1907272.

42. Segata N, Izard J, Waldron L *et al.* Metagenomic biomarker discovery and explanation. *Genome Biol* 2011;**12**:R60.

43. Gilbert J, Blaser MJ, Caporaso JG *et al.* Current understanding of the human microbiome. *Nat Med* 2018;**24**:392–400.

44. Bäumler AJ, Sperandio V. Interactions between the microbiota and pathogenic bacteria in the gut. *Nature* 2016;**535**:85–93.

45. Fierer N, Jackson RB. The diversity and biogeography of soil bacterial communities. *Proceedings of the National Academy of Sciences* 2006;**103**:626–31.

46. Cummings JH, Macfarlane GT. The control and consequences of bacterial fermentation in the human colon. *J Appl Bacteriol* 1991;**70**:443–59.

47. Duncan SH, Louis P, Thomson JM *et al.* The role of pH in determining the species composition of the human colonic microbiota. *Environmental Microbiology* 2009;**11**:2112–22.

48. Cremer J, Arnoldini M, Hwa T. Effect of water flow and chemical environment on microbiota growth and composition in the human colon. *Proceedings of the National Academy of Sciences* 2017;**114**:6438–43.

49. O'Toole PW, Marchesi JR, Hill C. Next-generation probiotics: the spectrum from probiotics to live biotherapeutics. *Nat Microbiol* 2017;**2**:17057.

50. EFSA Panel on Nutrition, Novel Foods and Food Allergens (NDA), Turck D, Bohn T *et al.* Safety of Clostridium butyricum TO-A as a novel food pursuant to Regulation (EU) 2015/2283. *EFSA Journal* 2025;**23**:e9371.

51. Sydney M. Finegold, Vera L. Sutter, and Glenn E. Mathisen. *CHAPTER 1 – Normal Indigenous Intestinal Flora*. New York: Academic Press, 1983.

52. Wang K, Wang K, Wang J *et al.* Protective Effect of Clostridium butyricum on Escherichia coli-Induced Endometritis in Mice via Ameliorating Endometrial Barrier and Inhibiting Inflammatory Response. *Microbiology Spectrum* 2022;**10**:e03286-22.

707 53. Chen D, Jin D, Huang S *et al. Clostridium butyricum*, a butyrate-producing probiotic, inhibits intestinal tumor
708 development through modulating Wnt signaling and gut microbiota. *Cancer Letters* 2020;**469**:456–67.

709 54. Liu P, Liu Z, Wang J *et al.* Immunoregulatory role of the gut microbiota in inflammatory depression. *Nat*
710 *Commun* 2024;**15**:3003.

711 55. Seki H, Shiohara M, Matsumura T *et al.* Prevention of antibiotic-associated diarrhea in children by Clostridium
712 butyricum MIYAIRI. *Pediatrics International* 2003;**45**:86–90.

713 56. Li H, Ma X, Li Y *et al.* The metagenomic and metabolomic profile of the gut microbes in Chinese full-term and
714 late preterm infants treated with Clostridium butyricum. *Sci Rep* 2023;**13**:18775.

715 57. Mukhopadhya I, Louis P. Gut microbiota-derived short-chain fatty acids and their role in human health and
716 disease. *Nat Rev Microbiol* 2025;**23**:635–51.

717 58. Shealy NG, Yoo W, Byndloss MX. Colonization resistance: metabolic warfare as a strategy against pathogenic
718 Enterobacteriaceae. *Current Opinion in Microbiology* 2021;**64**:82–90.

719 59. Raulo A, Bürkner P-C, Finerty GE *et al.* Social and environmental transmission spread different sets of gut
720 microbes in wild mice. *Nat Ecol Evol* 2024;**8**:972–85.

721 60. Eberl C, Weiss AS, Jochum LM *et al. E. coli* enhance colonization resistance against *Salmonella* Typhimurium
722 by competing for galactitol, a context-dependent limiting carbon source. *Cell Host & Microbe* 2021;**29**:1680-
723 1692.e7.

724 61. Felsenstein J. Phylogenies and the Comparative Method. *The American Naturalist* 1985;**125**:1–15.

725 62. Leon-Sampedro R, Boumasmoud M, Reichlin M *et al.* Multi-layered ecological interactions determine growth
726 of clinical antibiotic-resistant strains within human microbiomes. *bioRxiv* 2024:2024–11.

727 63. Herlemann DP, Labrenz M, Jürgens K *et al.* Transitions in bacterial communities along the 2000 km salinity
728 gradient of the Baltic Sea. *ISME J* 2011;**5**:1571–9.

729 64. Callahan BJ, McMurdie PJ, Rosen MJ *et al.* DADA2: High resolution sample inference from Illumina amplicon
730 data. *Nat Methods* 2016;**13**:581–3.

731 65. Callahan BJ, Sankaran K, Fukuyama JA *et al.* Bioconductor Workflow for Microbiome Data Analysis: from raw
732 reads to community analyses. *F1000Res* 2016;**5**:1492.

733 66. Hong Nhung P, Ohkusu K, Mishima N *et al.* Phylogeny and species identification of the family
734 *Enterobacteriaceae* based on *dnaJ* sequences. *Diagnostic Microbiology and Infectious Disease* 2007;**58**:153–61.

735 67. Hu D, Fuller NR, Caterson ID *et al.* Single-gene long-read sequencing illuminates Escherichia coli strain
736 dynamics in the human intestinal microbiome. *Cell Reports* 2022;**38**:110239.

737 68. Ruppé E, Lixandru B, Cojocaru R *et al.* Relative Fecal Abundance of Extended-Spectrum-β-Lactamase-
738 Producing Escherichia coli Strains and Their Occurrence in Urinary Tract Infections in Women. *Antimicrob Agents*
739 *Chemother* 2013;**57**:4512–7.

740 69. Chang AC, Cohen SN. Construction and characterization of amplifiable multicopy DNA cloning vehicles
741 derived from the P15A cryptic miniplasmid. *Journal of Bacteriology* 1978;**134**:1141–56.

742 70. Kiss J, Szabó M, Hegyi A *et al.* Identification and Characterization of oriT and Two Mobilization Genes
743 Required for Conjugative Transfer of Salmonella Genomic Island 1. *Front Microbiol* 2019;**10**:457.

744 71. Aranda-Díaz A, Willis L, Nguyen TH *et al.* Assembly of stool-derived bacterial communities follows "early-
745 bird" resource utilization dynamics. *Cell Systems* 2025;**16**:101240.

746 72. Arnoldini M, Sharma R, Moresi C *et al.* Quantifying the varying harvest of fermentation products from the
747 human gut microbiota. *Cell* 2025;**188**:5332-5342.e16.

748 73. Chure G, Cremer J. hplc-py: A Python Utility For Rapid Quantification of Complex Chemical Chromatograms.
749 *Journal of Open Source Software* 2024;**9**:6270.